Electronic Band Structure and Madelung Potential Study of the Nickelates La_2NiO_4, $La_3Ni_2O_7$, and $La_4Ni_3O_{10}$

D.-K. Seo,[†] W. Liang,[†] M.-H. Whangbo,*[,†] Z. Zhang,[‡] and M. Greenblatt*[,‡]

Departments of Chemistry, North Carolina State University, Raleigh, North Carolina 27695-8204, and Rutgers—The State University of New Jersey, Piscataway, New Jersey 08855

Received April 5, 1996[⊗]

Tight-binding electronic band structures and Madelung potentials were calculated for La_2NiO_4, $La_3Ni_2O_7$, and $La_4Ni_3O_{10}$ to examine why a metal-to-metal transition occurs in the nickelate $Ln_4Ni_3O_{10}$ (Ln = La, Nd, Pr). $La_4Ni_3O_{10}$ and $La_3Ni_2O_7$ are each found to have two hidden one-dimensional (1D) Fermi surfaces, which suggests that both compounds should possess a charge density wave instability. Factors leading to hidden 1D Fermi surfaces in the e_g block bands of the nickelates were discussed.

Introduction

The structures of ternary nickelates $Ln_{n+1}Ni_nO_{3n+1}$ (Ln = La for $n = 1, 2$; Ln = La, Pr, Nd for $n = 3$)[1] are similar to those of the Ruddlesden−Popper series $Sr_{n+1}Ti_nO_{3n+1}$.[2] In these nickelates, n consecutive perovskite layers, $(LaNiO_3)_n$, alternate with rock salt layers, LaO, along the crystallographic c direction so their formulas can be written as $(LnO)(LnNiO_3)_n$ (Figure 1). The $n = \infty$ member of this series corresponds to the three-dimensional perovskite $LnNiO_3$ (Ln = Sm, Nd, Pr, La).[3] The nickelates commonly possess oxygen atom deficiency, which affects their transport properties. Recently, the electrical and magnetic properties of La_2NiO_4,[4,5] $La_3Ni_2O_7$,[4,6] $Ln_4Ni_3O_{10}$ (Ln = Pr, Nd, La),[4,7] and $LnNiO_3$ (Ln = Sm, Nd, Pr, La)[3,4] have been the focus of substantial interest. The $n = 1$ member La_2NiO_4 is a magnetic semiconductor[8] and was examined by several electronic band structure calculations.[9] As the temperature is lowered, the $n = \infty$ member $LnNiO_3$ (Ln = Sm, Nd, Pr) undergoes a metal-to-insulator transition (403, 201, and 135 K for Ln = Sm, Nd, and Pr, respectively) whereas $LaNiO_3$ remains metallic.[3c] An electronic band structure study of $LaNiO_3$ was reported.[10] With decreasing temperature, $Ln_4Ni_3O_{10}$ (Ln = Pr, Nd, La) undergoes a metal-to-metal phase transition around 150−160 K[7] while $La_3Ni_2O_7$ remains metallic.[4,6] So far, no electronic band structure study has been reported for $La_3Ni_2O_7$ and $Ln_4Ni_3O_{10}$.

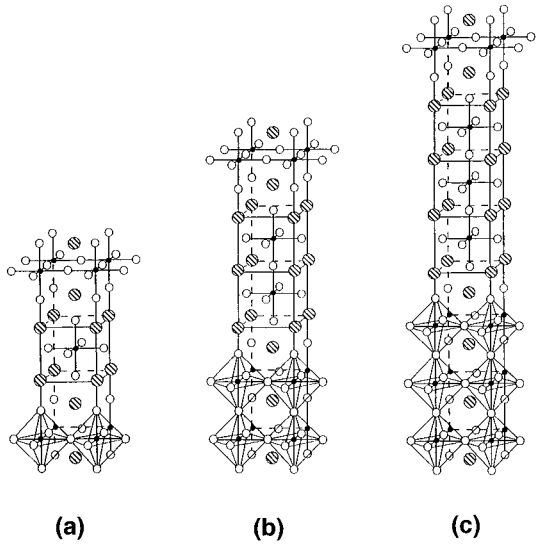

Figure 1. Perspective views of the crystal structures of (a) La_2NiO_4, (b) $La_3Ni_2O_7$, and (c) $La_4Ni_3O_{10}$. The small (black), medium (white), and large (hatched) circles refer to Ni, O, and La atoms, respectively.

Metal-to-insulator and metal-to-metal transitions are frequently observed for one-dimensional (1D) metals[11] because the nesting of their Fermi surfaces leads to a charge density wave (CDW) instability.[12] The Fermi surface of a partially filled band refers to the boundaries separating the occupied and unoccupied wave vectors of the band. The Fermi surface of a 1D band consists of parallel lines perpendicular to the direction

[†] North Carolina State University.
[‡] Rutgers—The State University of New Jersey.
[⊗] Abstract published in *Advance ACS Abstracts,* October 1, 1996.

(1) (a) Sepannen, M. *Scand. J. Metall.* **1979**, *8*, 191. (b) Brisi, J. C.; Vallino, M.; Abbattista, F. *J. Less-Common Met.* **1981**, *79*, 215. (c) Drenan, J.; Tavares, C. P.; Steele, B. C. H. *Mater. Res. Bull.* **1982**, *17*, 621. (d) Odier, P.; Nigara, Y.; Coutures, J.; Sayer, M. *J. Solid State Chem.* **1985**, *56*, 32.
(2) Ruddlesden, S. N.; Popper, P. *Acta Crystallogr.* **1958**, *11*, 54.
(3) (a) Vassiliou, J. K.; Hornbostel, M.; Ziebarth, R.; DiSalvo, F. J. *J. Solid State Chem.* **1989**, *81*, 208. (b) Lacorre, P.; Torrance, J. B.; Pannetier, J.; Nazzal, A. I.; Wang, P. W.; Huang, T. C. *J. Solid State Chem.* **1991**, *91*, 225. (c) Torrance, J. B.; Lacorre, P.; Nazzal, A. I.; Ansaldo, E. J.; Niedermayer, Ch. *Phys. Rev. B* **1992**, *45*, 8209. (d) Sreedhar, K.; Honig, J. M.; Darwin, M.; McElfresh, M.; Shand, P. M.; Xu, J.; Crooker, B. C.; Spalek, J. *Phys. Rev. B* **1992**, *46*, 6382. (e) Granados, X.; Fontcuberta, J.; Obradors, X.; Manosa, Ll.; Torrance, J. B. *Phys. Rev. B* **1993**, *48*, 11666. (f) Canfield, P. C.; Thompson, J. D.; Cheong, S.-W.; Rupp, L. W. *Phys. Rev. B* **1993**, *47*, 12357.
(4) Sreedhar, K.; McElfresh, M.; Perry, D.; Kim, D.; Metcalf, P.; Honig, J. M. *J. Solid State Chem.* **1994**, *110*, 208.
(5) (a) Rao, C. N. R.; Buttrey, D.; Otsuka, N.; Ganguly, P.; Harrison, H. R.; Sandberg, C. J.; Honig, J. M. *J. Solid State Chem.* **1984**, *51*, 266. (b) Singh, K. K.; Ganguly, P.; Goodenough, J. B. *J. Solid State Chem.* **1984**, *52*, 254. (c) Ganguly, P.; Rao, C. N. R. *Mater. Res. Bull.* **1973**, *8*, 405. (d) Sayer, M.; Odier, P. *J. Solid State Chem.* **1987**, *67*, 26.
(6) Zhang, Z.; Greenblatt, M.; Goodenough, J. B. *J. Solid State Chem.* **1994**, *108*, 402.
(7) (a) Lavrova, O. A.; Somenkov, V. A.; Tkalich, A. K.; Shulshtein, S. Sh.; Damm, I. D.; Ivanov-Smolenskii, G. A. *Superconductivity* **1991**, *4*, 1743. (b) Tkalich, A. K.; Glazkov, V. P.; Smolenskii, V. A.; Shulshtein, S. Sh.; Karkin, A. E.; Mirmelshtein, A. V. *Supercond.* **1991**, *4*, 2280. (c) Zhang, Z.; Greenblatt, M. *J. Solid State Chem.* **1995**, *117*, 236.
(8) (a) Wang, X.-L.; Stassis, C.; Johnston, D. C.; Leung, T. C.; Ye, J.; Harmon, B. N.; Lander, G. H.; Schultz, A. J.; Loong, C.-K.; Honig, J. M. *Phys. Rev. B* **1992**, *45*, 5645. (b) Wang, X.-L.; Stassis, C.; Johnston, D. C.; Leung, T. C.; Ye, J.; Harmon, B. N.; Lander, G. H.; Schultz, A. J.; Loong, C.-K.; Honig, J. M. *J. Appl. Phys.* **1991**, *69*, 4860. (c) Lander, G. H.; Brown, P. J.; Spalek, J.; Honig, J. M. *Phys. Rev. B* **1989**, *40*, 4463.
(9) (a) Guo, G. Y.; Temmerman, W. M. *J. Phys. C: Solid State Phys.* **1988**, *21*, L803. (b) Takegahara, K.; Kasuya, T. *Solid State Commun.* **1989**, *70*, 641. (c) Szpunar, B.; Smith, V. H., Jr.; Spalek, J. *Physica C* **1989**, *161*, 503. (d) de la Mora, P.; de Teresa, C.; Vincente, L. *Mater. Res. Soc. Symp. Proc.* **1993**, *291*, 331. (e) Choisnet, J.; Evarestov, R. A.; Tupitsin, I. I.; Veryazov, V. A. *Phys. Status Solidi B* **1993**, *179*, 441.
(10) Hamada, N. *J. Phys. Chem. Solids* **1993**, *54*, 1157.

S0020-1669(96)00379-5 CCC: $12.00

of the band dispersion. When a piece of the Fermi surface is superposed onto another piece by a translational vector **q**, it is said that the Fermi surface is nested by **q**. For a solid with the direct **R**, the CDW (i.e., periodic charge density modulation) associated with the nesting vector **q** is described by $\cos(\mathbf{q}\cdot\mathbf{R})$. A CDW instability in solids is analogous to a first-order Jahn−Teller instability that occurs in molecules with partially filled degenerate levels.[12]

A CDW instability is also found for certain two-dimensional (2D) metals whose Fermi surfaces are well described by a superposition of several 1D Fermi surfaces [e.g., Magnéli phase Mo_4O_{11}, purple bronze KMo_6O_{17}, and monophosphate tungsten bronzes $(PO_2)_4(WO_3)_m(WO_3)$].[12,13] Such 1D Fermi surfaces, as obtained by decomposing 2D Fermi surfaces, are referred to as hidden 1D Fermi surfaces. The metal atoms of these compounds are located at the octahedral sites, and their partially filled bands are t_{2g} block bands. The hidden 1D Fermi surfaces result because interactions between the t_{2g} orbitals of metal atoms are strong only when their orbital lobes are contained within a same plane.

With the average oxidation state of Ni ranging from +2 (for $n = 1$) to +3 (for $n = \infty$), the partially filled bands of $(LnO)(LnNiO_3)_n$ and $LnNiO_3$ are derived from the e_g orbitals of their NiO_6 octahedra. Provided that the in-plane Ni−O bonds of an NiO_6 octahedron are positioned along the x and y axes, the e_g orbitals are given by z^2 (a short notation for $3z^2 - r^2$)[14] and $x^2 - y^2$. For a perovskite layer $(NiO_3)_n$ ($n \leq 3$), one might consider that the bands derived from the $x^2 - y^2$ orbitals will be more dispersive than those derived from the z^2 orbitals, and both sets of bands will have 2D character. This reasoning does not explain why $Ln_4Ni_3O_{10}$ shows such a resistivity anomaly as is often observed for 1D metals. Therefore, it is necessary to investigate whether the anomaly results from hidden 1D Fermi surfaces and, if so, how the e_g orbital bands give rise to 1D bands. It is also important to examine if the electronic structure of $La_3Ni_2O_7$ has a feature identical with that of $Ln_4Ni_3O_{10}$ causing the resistivity anomaly. These questions were probed in the present work on the basis of the electronic structures of La_2NiO_4, $La_3Ni_2O_7$, and $La_4Ni_3O_{10}$ that were calculated using the extended Hückel tight binding (EHTB) method.[15] The atomic parameters employed for our EHTB calculations are summarized in Table 1.

Because of electron correlation it is generally difficult to predict whether or not late transition metal oxides are metallic by any electronic band structure calculations including first-principle ones.[16−18] For example, in disagreement with the experimental results,[8] La_2NiO_4 is predicted to be metallic by most electronic band structure calculations.[9] The primary focus of our study is on $La_4Ni_3O_{10}$ for which a one-electron electronic structure description is considered to be adequate.[4] In EHTB electronic band structure calculations for transition metal oxides, electrostatic Coulombic interactions between the ions are not well described. This is in part responsible for why EHTB calculations show a sizable energy gap between the p and d block bands of late transition metal oxides whereas first-principle calculations do not. A recent study indicates that electron correlation in transition metal oxides can be reasonably well estimated in terms of gas phase ionization potentials and bare electrostatic Coulombic interactions.[19] In the present work, electrostatic Coulombic interactions in the three oxides La_2NiO_4, $La_3Ni_2O_7$, and $La_4Ni_3O_{10}$ are examined in terms of their Madelung potentials calculated using the PACK program.[20]

Table 1. Exponents, ζ_i, and Valence Shell Ionization Potentials, H_{ii} of Slater-type Orbitals, χ_i, Used for EHTB Calculations[a]

atom	χ_i	H_{ii} (eV)	ζ_i	c_1[b]	ζ_i'	c_2[b]
Ni	4s	−9.17	2.10			
Ni	4p	−5.15	2.10			
Ni	3d	−13.4	5.75	0.5857	2.2	0.5902
O	2s	−32.3	2.275			
O	2p	−14.8	2.275			

[a] H_{ii}'s are the diagonal matrix elements $\langle\chi_i|H^{\text{eff}}|\chi_i\rangle$, where H^{eff} is the effective Hamiltonian. In our calculations of the off-diagonal matrix elements $H^{\text{eff}} = \langle\chi_i|H^{\text{eff}}|\chi_j\rangle$, the weighted formula was used (Ammeter, J.; Bürgi, H.-B.; Thibeault, J.; Hoffmann, R. *J. Am. Chem. Soc.* **1978**, *100*, 3686). [b] Contraction coefficients used in the double-zeta Slater-type orbital.

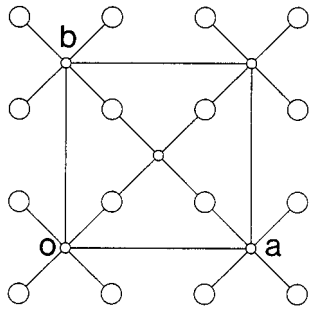

Figure 2. Arrangement of a single perovskite layer in $La_3Ni_2O_7$ and $Ln_4Ni_3O_{10}$ showing only the Ni and O_{eq} atoms. The small and large circles represent the Ni and O_{eq} atoms, respectively.

Electronic Structures of $La_3Ni_2O_7$ and $La_4Ni_3O_{10}$

As depicted in Figure 2, the unit cell of each perovskite layer in $La_3Ni_2O_7$ and $La_4Ni_3O_{10}$ has two Ni atoms, and the in-plane Ni−O bonds run along the directions diagonal to the repeat vectors **a** and **b** (i.e., along the **a** + **b** and −**a** + **b** directions). The unit cells of $La_3Ni_2O_7$ and $La_4Ni_3O_{10}$ are each twice the formula units in size so that, per unit cell, there are six electrons to fill the eight e_g block bands of $La_3Ni_2O_7$ and eight electrons to fill the 12 e_g block bands of $La_4Ni_3O_{10}$. Later in our discussion, it is important to distinguish the in-plane and out-of-plane Ni−O bonds of each perovskite layer. In this work, the oxygen atoms forming the in-plane and out-of-plane Ni−O bonds will be referred to as O_{eq} (i.e., equatorial oxygen) and O_{ax} (i.e., axial oxygen), respectively. The lengths of the Ni−O_{eq} and Ni−O_{ax} bonds found for La_2NiO_4, $La_3Ni_2O_7$, and $La_4Ni_3O_{10}$ are listed in Table 2.

(11) For reviews, see: (a) *Electronic Properties of Inorganic Quasi-One-Dimensional Compounds*; Monceau, P., Ed.; Reidel: Dordrecht, The Netherlands, 1985; parts I and II. (b) *Crystal Chemistry and Properties of Materials with Quasi-One-Dimensional Structures*; Rouxel, J., Ed.; Reidel: Dordrecht, The Netherlands, 1986. (c) *Structure Phase Transitions in Layered Transition Metal Compounds*; Motizuki, K., Ed.; Reidel: Dordrecht, The Netherlands, 1986. (d) *Low-Dimensional Electronic Properties of Molybdenum Bronzes and Oxides*; Schlenker, C., Ed.; Kluwer Academic Publ.: Dordrecht, The Netherlands, 1989. (e) Pouget, J. P. In *Semiconductors and Semimetals*; Conwell, E., Ed.; Academic Press: New York, 1988; Vol. 27, p 87. (f) Friend, H.; Yoffe, A. D. *Adv. Phys.* **1987**, *36*, 1. (g) Withers, R. L.; Wilson, J. A. *J. Phys. C: Solid State Phys.* **1986**, *19*, 4809.

(12) (a) Whangbo, M.-H.; Canadell, E. *J. Am. Chem. Soc.* **1992**, *114*, 9587. (b) Canadell, E.; Whangbo, M.-H. *Chem. Rev.* **1991**, *91*, 965.

(13) (a) Whangbo, M.-H.; Canadell, E.; Foury, P.; Pouget, J.-P. *Science* **1991**, *252*, 96. (b) Canadell, E.; Whangbo, M.-H. *Int. J. Mod. Phys. B* **1993**, *7*, 4005. (c) Whangbo, M. -H.; Ren, J.; Liang, W.; Canadell, E.; Pouget, J. -P.; Ravy, S.; Williams, J. M.; Beno, M. A. *Inorg. Chem.* **1992**, *31*, 4169. (d) Rousseau, R.; Palacin, M. R.; Gomez-Romero, P.; Canadell, E. *Inorg. Chem.* **1996**, *35*, 1179.

(14) Albright, T. A.; Burdett, J. K.; Whangbo, M.-H. *Orbital Interactions in Chemistry*; Wiley: New York, 1985.

(15) Whangbo, M.-H.; Hoffmann, R. *J. Am. Chem. Soc.* **1978**, *100*, 6093.

(16) Brandow, B. H. *Adv. Phys.* **1977**, *26*, 651.

(17) (a) Zaanen, J.; Sawatzky, G. A.; Allen, J. W. *Phys. Rev. Lett.* **1985**, *55*, 418. (b) Zaanen, J.; Sawatzky, G. A. *J. Solid State Chem.* **1990**, *88*, 8.

(18) Czyzyk, M. T.; Sawatzky, G. A. *Phys. Rev. B* **1994**, *49*, 14211.

(19) Torrance, J. B.; Lacorre, P.; Asavaroengchai, C.; Metzger, R. M. *Physica C* **1991**, *182*, 351.

(20) Liang, W.; Whangbo, M.-H. Unpublished work.

Table 2. Ni−O Bond Lengths and Madelung Potentials (V_M) at the Nickel and Oxygen Atoms in La_2NiO_4, $La_3Ni_2O_7$, and $La_4Ni_3O_{10}$

compound	V_M (|e|/Å) oxygen		V_M (|e|/Å) nickel		Ni−O (Å)
La_2NiO_4	O_{eq}	1.335	Ni	−1.899	Ni−O_{eq} = 1.935
	O_{ax}	1.556			Ni−O_{ax} = 2.243
$La_3Ni_2O_7$	O_{eq}	1.423	Ni	−2.462	Ni−O_{eq} = 1.917
	O_{ax}(o)[a]	1.536			Ni−O_{ax}(o) = 1.962[b]
	O_{ax}(i)[a]	1.357			Ni−O_{ax}(i) = 1.978[b]
$La_4Ni_3O_{10}$	O_{eq}(o)	1.452	Ni(o)	−2.547	Ni−O_{eq}(o) = 1.923
	O_{eq}(i)	1.415	Ni(i)	−2.592	Ni−O_{eq}(i) = 1.923
	O_{ax}(o)	1.617			Ni−O_{ax}(o) = 1.957
	O_{ax}(i)	1.425			Ni−O_{ax}(i) = 1.929

[a] When there are nonequivalent Ni−O_{ax} bonds and nonequivalent Ni atoms, the symbols (o) and (i) refer to the outer and inner parts of the perovskite layer structures, respectively. [b] The crystal structure of ref 6 shows that the two Ni−O_{ax} bond lengths are quite unsymmetrical, i.e., Ni−O_{ax}(o) = 1.906 Å and Ni−O_{ax}(i) = 1.993 Å. The values listed in this table are obtained by using the fractional coordinates of (0, 0, 0.0964) for Ni and (0, 0, 0.192) for O(2), both of which are equally valid within the standard deviation. These fractional coordinates were for the electronic band structure calculations of $La_3Ni_2O_7$.

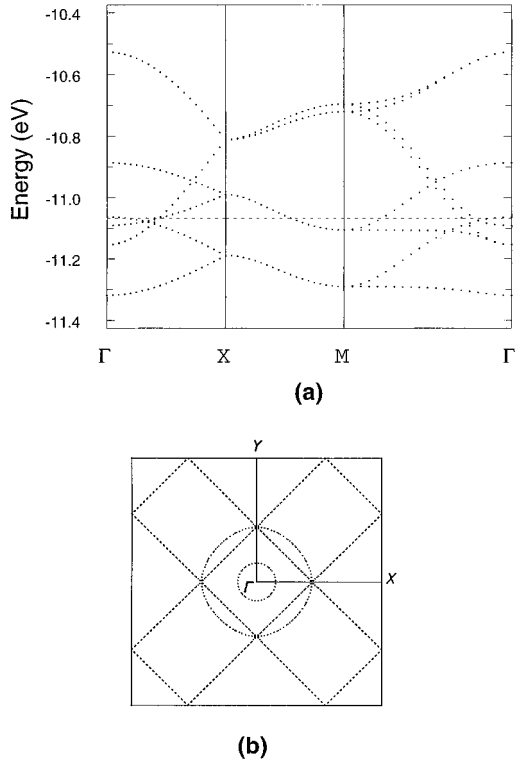

Figure 3. Electronic band structure calculated for $La_3Ni_2O_7$: (a) dispersion relations of the e_g-block bands; (b) Fermi surfaces associated with the partially filled e_g block bands. Γ = (0, 0), X = (**a***/2, 0), Y = (0, **b***/2), and M = (**a***/2, **b***/2).

The dispersion relations of the e_g block bands calculated for $La_3Ni_2O_7$ and $La_4Ni_3O_{10}$ are presented in Figures 3a and 4a, respectively, where the dashed lines refer to the Fermi levels. The Fermi surfaces associated with the partially filled bands of $La_3Ni_2O_7$ and $La_4Ni_3O_{10}$ are shown in Figures 3b and 4b, respectively. A striking feature of the Fermi surfaces of $La_4Ni_3O_{10}$ (Figure 4b) is that there exist nearly parallel lines (i.e., 1D Fermi surfaces) perpendicular to each of the two Ni−O_{eq} bond directions (i.e., along the **a*** + **b*** and −**a*** + **b*** directions, which are identical with the **a** + **b** and −**a** + **b** directions, respectively). This means that there is one 1D band dispersive along **a** + **b** and another 1D band dispersive along −**a** + **b**. As depicted in Figure 5, the Fermi surfaces of these two 1D bands are simultaneously nested by the vector $\mathbf{q_a}$ = 0.30**a*** or $\mathbf{q_b}$ = 0.30**b***. The CDW instability associated with

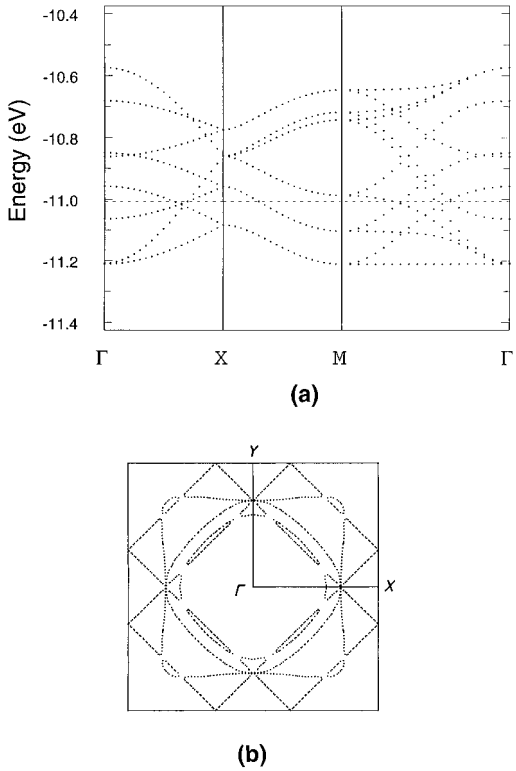

Figure 4. Electronic band structure calculated for $La_4Ni_3O_{10}$: (a) dispersion relations of the e_g block bands; (b) Fermi surfaces associated with the partially filled e_g block bands. Γ = (0, 0), X = (**a***/2, 0), Y = (0, **b***/2), and M = (**a***/2, **b***/2).

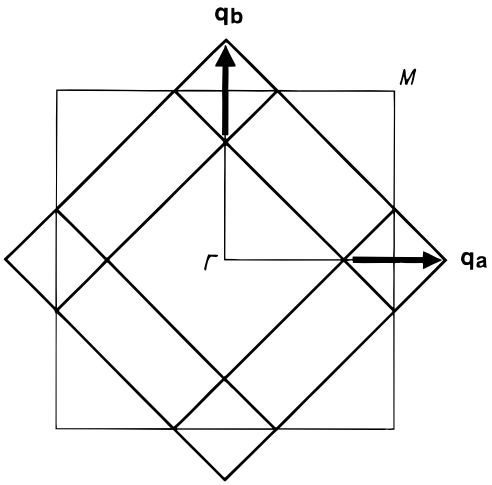

Figure 5. Schematic drawing that shows the common nesting vectors $\mathbf{q_a}$ = (0.3**a***, 0) and $\mathbf{q_b}$ = (0, 0.3**b***) for the two hidden 1D Fermi surfaces found for $La_4Ni_3O_{10}$. Γ = (0, 0) and M = (**a***/2, **b***/2).

these nesting vectors is probably responsible for the metal-to-metal transition observed for $Ln_4Ni_3O_{10}$ around 150−160 K.

The Fermi surfaces of $La_3Ni_2O_7$ (Figure 3b) also possess two 1D Fermi surfaces perpendicular to each of the two Ni−O_{eq} bond directions, and the two surfaces are simultaneously nested by the vector $\mathbf{q_a}$ = 0.44**a*** or $\mathbf{q_b}$ = 0.44**b***. Thus, a CDW phenomenon is predicted for $La_3Ni_2O_7$, although it has not yet been observed.[6] The latter may be due to a poor sample quality because, in the case of $La_4Ni_3O_{10}$,[4,7] it was found to depend on the quality of the samples as to whether they exhibit a metal-to-metal transition.

Cause for Hidden 1D Fermi Surfaces

Let us now discuss how the e_g block bands of $La_3Ni_2O_7$ and $La_4Ni_3O_{10}$ possess two 1D bands, each dispersive along one of

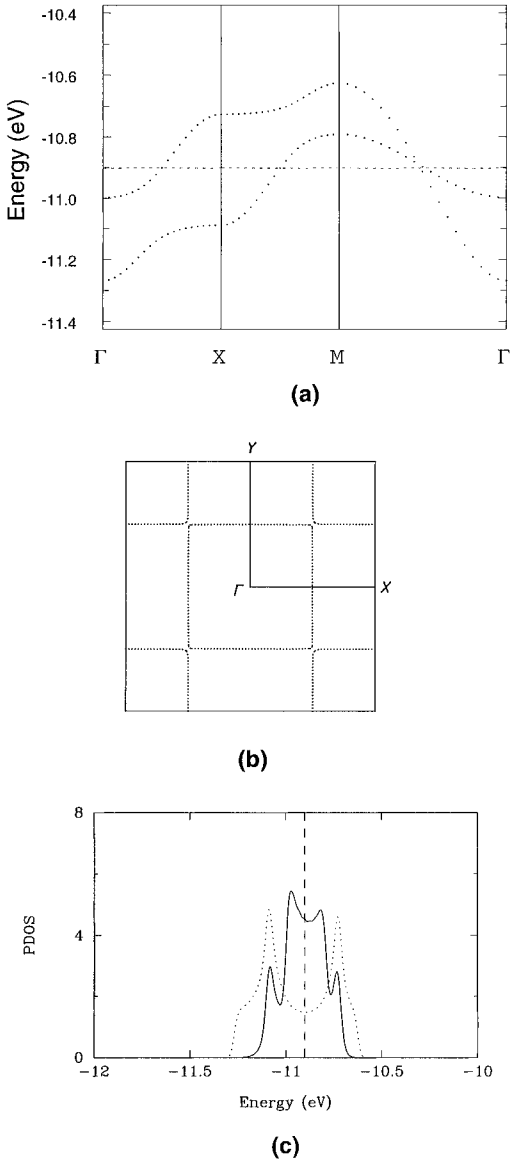

Figure 6. Electronic structure of the perovskite NiO_4^{6-} lattice with $Ni-O_{ax} = Ni-O_{eq} = 1.93$ Å: (a) dispersion relations of the e_g block bands; (b) Fermi surfaces associated with the partially filled e_g block bands; (c) PDOS plots of the Ni z^2 and $x^2 - y^2$ orbitals (solid and dotted lines, respectively) calculated for the e_g-block bands. $\Gamma = (0, 0)$, $X = (\mathbf{a}^*/2, 0)$, $Y = (0, \mathbf{b}^*/2)$, and $M = (\mathbf{a}^*/2, \mathbf{b}^*/2)$.

the two $Ni-O_{eq}$ bond directions. For this purpose, we calculate the e_g block bands of a single perovskite layer NiO_4^{6-}, which simulates the e_g block bands of La_2NiO_4. We arrange the $Ni-O_{eq}$ bonds of this layer along the x and y axes, so the e_g block levels are given by the z^2 and $x^2 - y^2$ orbitals. In a perovskite layer NiO_4^{6-} there are two electrons per unit cell to fill the two e_g block bands so that the e_g block bands as a whole are half-filled. Figure 6a shows the dispersion relations of the e_g block bands calculated for the ideal perovskite NiO_4^{6-} layer made up of regular NiO_6 octahedra ($Ni-O_{ax} = Ni-O_{eq} = 1.93$ Å). The Fermi surfaces associated with these bands (Figure 6b) are essentially decomposed into two hidden 1D Fermi surfaces, each perpendicular to one of the two $Ni-O_{eq}$ bond directions. In addition, the 1D band responsible for each 1D Fermi surface is half-filled because the parallel lines of each Fermi surface are separated by $0.5\mathbf{a}^*$ or $0.5\mathbf{b}^*$. The contributions of the Ni z^2 and $x^2 - y^2$ orbitals to the e_g block bands can be examined in terms of projected density of state (PDOS) plots. Figure 6c shows that the "z^2" and "$x^2 - y^2$" bands (i.e., the PDOS plots representing the z^2 and $x^2 - y^2$ orbital contributions, respectively) overlap nearly symmetrically around the Fermi level.

All of the above observations can be explained if, in the region of the Fermi level, the z^2 and $x^2 - y^2$ orbitals are linearly combined to form hybridized orbitals $z^2 - y^2$ and $z^2 - x^2$. Namely,

$$(3z^2 - r^2) + (x^2 - y^2) \propto z^2 - y^2$$

$$(3z^2 - r^2) - (x^2 - y^2) \propto z^2 - x^2$$

With the orbitals of the bridging ligands O_{eq}, the $z^2 - y^2$ orbital of the Ni atoms make a sigma overlap along the y axis direction but no overlap along the x axis direction. Therefore, the $z^2 - y^2$ orbitals lead to a 1D band dispersive only along the y axis direction. Likewise, the $z^2 - x^2$ orbitals lead to a 1D band dispersive only along the x axis direction. This explains why the Fermi surfaces of Figure 6b are composed of two 1D surfaces. To produce the two 1D Fermi surfaces found for $La_3Ni_2O_7$ and $La_4Ni_3O_{10}$, a d orbital hybridization similar to that discussed above must occur in two of their e_g block bands.

It is important to recognize why such a d orbital hybridization should occur. The d block bands of a solid are antibonding between the metal and ligand atoms.[14] In the d block bands of a solid made up of ML_n polyhedra (M = transition metal, L = ligand atoms such as oxygen, chalcogen, and halogen) by sharing their corners, edges, or faces, a certain set of ligand atoms cannot contribute their orbitals for certain values of the wave vector.[12] For these wave vectors, therefore, the site symmetry of a metal atom M in the solid is lower than that of an isolated ML_n polyhedron. This makes the d block orbitals of an ML_n polyhedral unit mix together (i.e., hybridize) to form lower-lying d block orbitals.

Madelung Potentials and Overlap between the e_g Block Bands

The extent of hybridization between the z^2 and $x^2 - y^2$ orbitals depends on how the z^2 and $x^2 - y^2$ bands overlap in the region of the Fermi level. To illustrate this point, results of our calculations for the NiO_4^{6-} layer with $Ni-O_{ax} = 1.96$ Å and $Ni-O_{eq} = 1.93$ Å are summarized in Figure 7 When the $Ni-O_{ax}$ bond is lengthened, the z^2 band is lowered with respect to the $x^2 - y^2$ band, which makes the two bands overlap unsymmetrically around the Fermi level (Figure 7c). As a consequence, the orbital hybridization around the Fermi level is not given by a 50:50 mixing of the z^2 and $x^2 - y^2$ orbitals, and the resulting Fermi surfaces (Figure 7b) are not well described as a superposition of two 1D Fermi surfaces. Our calculations of the NiO_4^{6-} layer (with $Ni-O_{eq}$ fixed at 1.93 Å) show that the overlap between the z^2 and $x^2 - y^2$ bands vanishes quickly as the $Ni-O_{ax}$ bond length is increased. For the case of $Ni-O_{ax} = 2.243$ Å and $N-O_{eq} = 1.935$ Å found for La_2NiO_4, the two bands are completely separated according to the present calculations (Figure 8a). This is understandable because the lengthening of the $Ni-O_{ax}$ bond reduces the extent of antibonding in the z^2 block level (Figure 9). However, there exists another factor affecting the overlap between the z^2 and $x^2 - y^2$ bands because, according to first-principle electronic structure calculations for the normal metallic state of La_2NiO_4,[9a] the z^2 and $x^2 - y^2$ bands still overlap considerably (Figure 8b). It is important to understand why this happens.

The O_{eq} and O_{ax} atoms of La_2NiO_4 are not equivalent and hence must have different potentials acting on them. This aspect is not reflected in EHTB calculations because the matrix elements of the effective Hamiltonian H^{eff} are not adjusted in a self-consistent manner. As already pointed out, the lengthening of the $Ni-O_{ax}$ bond lowers the z^2 level if the orbital character of O_{ax} remains the same as that of O_{eq}. The extent of antibonding in the $Ni-O_{ax}$ bond can remain substantial, even

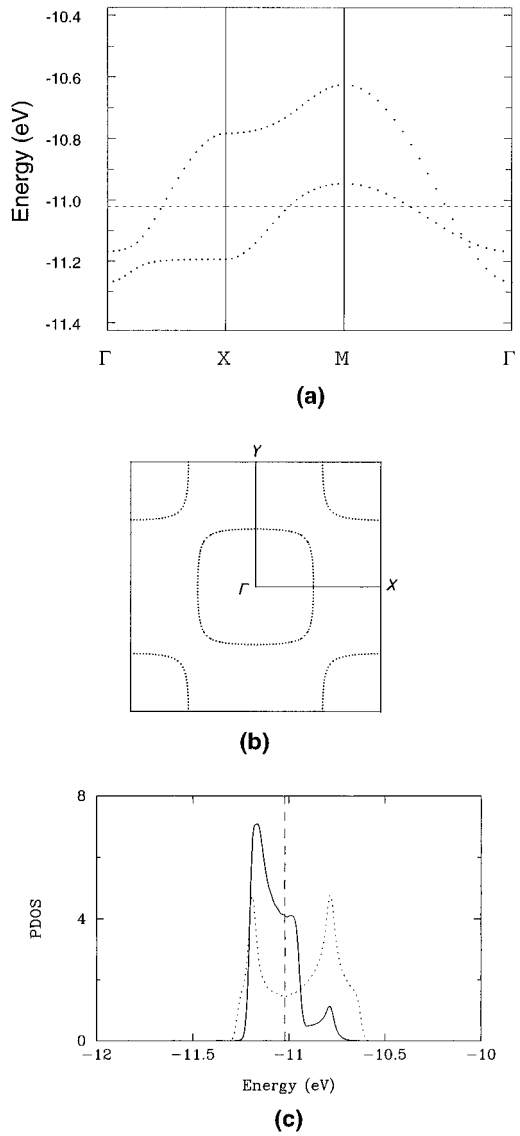

Figure 7. Electronic structure of the perovskite NiO_4^{6-} lattice with Ni−O_{ax} = 1.96 Å and Ni−O_{eq} = 1.93 Å: (a) dispersion relations of the e_g block bands; (b) Fermi surfaces associated with the partially filled e_g block bands. (c) PDOS plots of the Ni z^2 and $x^2 - y^2$ orbitals (solid and dotted lines, respectively) calculated for the e_g-block bands. Γ = (0, 0), X = (**a***/2, 0), Y = (0, **b***/2), and M = (**a***/2, **b***/2).

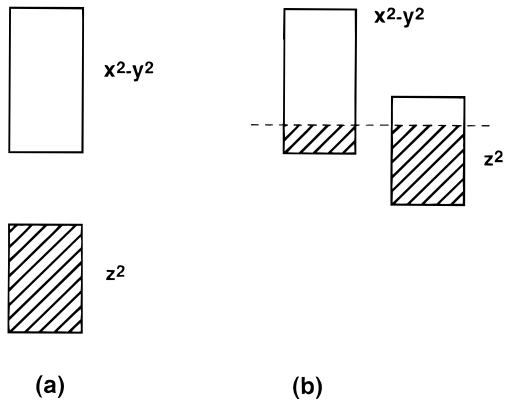

Figure 8. Schematic diagrams showing relative positions of z^2 and $x^2 - y^2$ bands calculated for the normal metallic state of La_2NiO_4: (a) EHTB calculation; (b) first principle calculation (ref 9a).

after the bond lengthening, if the orbitals of O_{ax} are more diffuse than those of O_{eq}. The more diffuse orbitals lead to a better overlap with the Ni d orbitals and enhance the extent of antibonding in the z^2 level, thereby diminishing the energy-lowering effect of the Ni−O_{ax} bond lengthening. The orbitals of O_{ax} can be more diffuse than those of O_{eq} if the effective potential acting on O_{ax} is more repulsive than that on O_{eq}. To test this idea, we used the PACK program[20] to calculate the Madelung potentials for the nickel and oxygen atom sites of La_2NiO_4 assuming the presence of Ni^{2+}, La^{3+}, and O^{2-} ions. Our results (Table 2) clearly confirm that the Madelung potential is more repulsive on O_{ax} than on O_{eq}, as suggested. Table 2 also lists the Madelung potentials calculated for $La_3Ni_2O_7$ and $La_4Ni_3O_{10}$. Compared with the case of La_2NiO_4, the Madelung potentials on the O_{eq} and O_{ax} atoms of $La_3Ni_2O_7$ and $La_4Ni_3O_{10}$ show much smaller differences. Thus, the results of our EHTB calculations concerning these nickelates are not expected to change substantially.

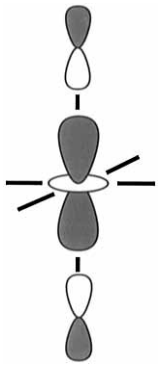

Figure 9. Schematic diagram showing the antibonding interaction in Ni−O_{ax} bonds in the z^2 block level of an NiO_6 octahedron.

Concluding Remarks

The resistivity anomaly observed for $La_4Ni_3O_{10}$ at around 150−160 K was examined on the basis of EHTB calculations. This system possesses two hidden 1D Fermi surfaces perpendicular to each of the Ni−O_{eq} bonds. The observed metal-to-metal transition is explained by a CDW instability associated with the common nesting vector of these 1D surfaces (0.3**a*** or 0.3**b***). $La_3Ni_2O_7$ also has two hidden 1D Fermi surfaces, which are commonly nested by a vector 0.44**a*** or 0.44**b***. Though not yet observed, $La_3Ni_2O_7$ is predicted to show a CDW instability.

The present study shows that the hidden 1D Fermi surfaces arise from the e_g block bands when the z^2 and $x^2 - y^2$ orbitals are hybridized to form $z^2 - x^2$ and $z^2 - y^2$ orbitals. Such a hybridization occurs when the z^2 and $x^2 - y^2$ bands overlap symmetrically around the Fermi level. The relative positions of the z^2 and $x^2 - y^2$ bands is affected by the bond length ratio Ni−O_{ax}/Ni−O_{eq} and also by the Madelung potentials acting on the O_{ax} and O_{eq} atoms.

A number of solids are made up of ML_n polyhedra by sharing their corners, edges, or faces. It is common to discuss the electronic structures of such solids from the viewpoint of the d block levels of an isolated ML_n polyhedron. It is important to note that this description becomes inadequate when a d orbital hybridization can generate lower-lying d levels than those expected from the d levels of an isolated ML_n polyhedron. This situation occurs in the e_g block bands of the nickelates as well as in the z^2 bands of 2H−TaS_2 (made up of TaS_6 trigonal prisms)[12a] and LaI_2 (made up of LaI_8 square prisms).[21]

Acknowledgment. This work was supported by the Office of Basic Energy Sciences, Division of Materials Sciences, U.S. Department of Energy, under Grant DE-FG05-86ER45259.

IC960379J

(21) Canadell, E.; Whangbo, M.-H. *Inorg. Chem.* **1994**, *33*, 287.